Nature. Author manuscript; available in PMC 2015 May 20.

Published in final edited form as:
Nature. 2014 November 20; 515(7527): 427–430. doi:10.1038/nature13715.

Structure of malaria invasion protein RH5 with erythrocyte basigin and blocking antibodies

Katherine E. Wright[1], **Kathryn A. Hjerrild**[2], **Jonathan Bartlett**[1], **Alexander D. Douglas**[2], **Jing Jin**[2], **Rebecca E. Brown**[2], **Joseph J. Illingworth**[2], **Rebecca Ashfield**[2], **Stine B. Clemmensen**[3], **Willem A. de Jongh**[3], **Simon J. Draper**[2], and **Matthew K. Higgins**[1]

[1]Department of Biochemistry, University of Oxford, South Parks Road, Oxford, OX1 3QU

[2]Jenner Institute, University of Oxford, Old Road Campus Research Building, Roosevelt Drive, Oxford, OX3 7DQ

[3]ExpreS[2]ion Biotechnologies, SCION-DTU Science Park, Agern Allé 1, DK-2970 Horsholm, Denmark

Invasion of host erythrocytes is essential to the life cycle of *Plasmodium* parasites and development of the pathology of malaria. The stages of erythrocyte invasion, including initial contact, apical reorientation, junction formation, and active invagination, are directed by coordinated release of specialised apical organelles and their parasite protein contents[1]. Among these proteins, and central to invasion by all species, are two parasite protein families, the reticulocyte-binding protein homologue (RH) and erythrocyte-binding like (EBL) proteins, that mediate host-parasite interactions[2]. RH5 from *Plasmodium falciparum* (PfRH5) is the only member of either family demonstrated to be necessary for erythrocyte invasion in all tested strains, through its interaction with the erythrocyte surface protein basigin (CD147, EMMPRIN)[3,4]. Indeed, antibodies targeting PfRH5 or basigin efficiently block parasite invasion *in vitro*[4-9], making PfRH5 an excellent vaccine candidate. Here we present crystal structures of PfRH5 in complex with basigin and two distinct inhibitory antibodies. PfRH5 adopts a novel fold in which two three-helical bundles come together in a kite-like architecture, presenting binding sites for basigin and inhibitory antibodies at one tip. This provides the first structural insight into erythrocyte binding by the *Plasmodium* RH protein family and identifies novel inhibitory epitopes to guide design of a new generation of vaccines against the blood-stage parasite.

Correspondence and requests for materials should be addressed to MKH (matthew.higgins@bioch.ox.ac.uk) and SD (simon.draper@ndm.ox.ac.uk).

Author contributions: KEW purified and crystallized the proteins, collected and analysed SAXS data, and performed SPR and AUC analysis. MKH and KEW prepared crystals for data collection and solved the structures. WAJ and SBC made S2 cell lines, and KAH and JJI purified proteins. ADD and JB provided hybridomas. JJ, REB and RA designed and performed parasite assays and ELISAs. KEW, MKH, and SJD designed the project, analysed the data, and wrote the paper.

Atomic coordinates and structure factors are deposited at the Protein Data Bank with accession codes 4U0Q, 4U0R and 4U1G.

The authors declare competing financial interests. ADD, JJI and SJD are named on patent applications relating to PfRH5 and/or other malaria vaccines. WAJ is named on patents relating to *Drosophila* S2 protein expression and is co-founder of ExpreS[2]ion Biotechnologies.

Europe PMC Funders Author Manuscripts

Each *Plasmodium* species contains at least one RH protein. These are often large, of low sequence complexity and with no homology to proteins of known structure. PfRH5 is unusual in being significantly shorter than its homologues (~60kDa for PfRH5 vs 200-375kDa for other RH proteins). It lacks their C-terminal transmembrane segment, but associates peripherally with the membrane and with PfRH5 interacting protein (PfRipr)[10]. Although it shares only ~20% pairwise sequence identity with other PfRH proteins[3,11], PfRH5 is remarkably conserved, with only five common non-synonymous single nucleotide polymorphisms (SNPs)[7,8,12]. Crucially, antibodies raised against one PfRH5 variant neutralise parasites of all tested heterologous strains, containing these and other less common SNPs[6,8], and anti-PfRH5 monoclonal antibodies that prevent parasite growth *in vitro* can directly block the PfRH5:basigin interaction[5]. Moreover, acquisition of anti-PfRH5 antibodies during natural infection correlates with clinical outcome and these antibodies can inhibit parasite growth *in vitro*[13]. These findings have generated intense excitement about PfRH5 as a next-generation blood-stage malaria vaccine target and emphasised the need for structural information to guide rational immunogen design.

Structural studies of PfRH5 required a protein construct lacking flexible regions but still capable of binding basigin. Long disordered regions were predicted within residues 1-140 and 248-296 (Extended Data Fig. 1a), and in cultured parasite lines, PfRH5 is processed by removal of the N-terminus to generate a ~45 kDa fragment[3,10]. We therefore designed PfRH5ΔNL, encompassing residues 140-526 but lacking 248-296, and showed it to bind basigin by surface plasmon resonance (SPR) with an affinity of 1.3 μM (Fig. 1C), comparable to the affinity of full-length PfRH5 for basigin (1.1μM)[4].

To ensure that PfRH5ΔNL contains epitopes required to elicit an inhibitory immune response, we raised rabbit polyclonal IgG and tested their ability to neutralise parasites by a growth-inhibitory activity (GIA) assay (Fig. 1D). IgG raised against PfRH5ΔNL protein showed a potent inhibitory effect, similar to that of IgG raised by immunisation of rabbits with viral vectors expressing full-length PfRH5[6], or full-length PfRH5 recombinant protein[8,9]. We also tested binding of PfRH5ΔNL to a panel of mouse monoclonal antibodies previously characterized for PfRH5 binding and growth-inhibitory activity[5]. PfRH5ΔNL bound to growth-inhibitory antibodies including QA1, QA5, and 9AD4, but not to non-inhibitory 4BA7 and RB3 (Extended Data Fig. 2). Thus, PfRH5ΔNL induces a growth-inhibitory immune response, and contains the epitopes targeted by inhibitory antibodies.

For structural studies, PfRH5ΔNL was mixed with basigin or fragments of growth-inhibitory monoclonal antibodies, 9AD4 or QA1. The complexes were trimmed using GluC protease and lysines chemically methylated before crystallisation. Crystals formed and data were collected to 3.1Å (PfRH5ΔNL:basigin), 2.3Å (PfRH5ΔNL:9AD4) and 3.1Å resolution (PfRH5ΔNL:QA1). Structures were determined using molecular replacement (Extended Data Table 1).

PfRH5 adopts a rigid, flat, ‘kite-shaped’ architecture with a pseudo-two-fold rotation symmetry and no similarity to known structures (Fig. 1A). Each half is predominantly built from a three helical bundle, with the outermost helices containing significant kinks or breaks. The N-terminal half begins with a short, two-stranded β-sheet that crosses the long

axis of the kite at its centre. This is followed by a single, short helix and two long, kinked helices connected by the truncated loop (containing 58 residues in full-length PfRH5). The C-terminal half is simpler, consisting of three long helices that span the entire length of the domain and finishing with a flexible C-terminus. One disulphide bond (C345-C351) stabilises the loop that links the two halves of the structure, while another links the second and third helices (C224-C317), leaving one unpaired cysteine (C329).

PfRH5 is predominantly rigid, with five copies in the three different crystal forms aligning with an rmsd of 0.9Å over 95% of residues (Extended Data Fig. 1b). Only the C-terminus (residue 496-end) and the loop linking helices 4 and 5 (residues 396-406) adopt different positions in different crystal forms. A molecular envelope derived from small angle X-ray scattering (SAXS) analysis of full-length PfRH5 in solution exhibits a similar flat structure (Fig. 1B, Extended Data Figure 3). This envelope is elongated relative to PfRH5ΔNL, most likely due to residues missing in this construct or not ordered in the crystal structure (22 residues at the C-terminus, the flexible loop, and perhaps part of the extended N-terminus).

As members of the *Plasmodium* RH family share little sequence identity, sequence alignments and structure-based threading were used to predict whether other members contain the PfRH5 fold. In each protein analysed (*P. falciparum* RH1, RH2a, RH2b, RH3 and RH4; *P. vivax* RBP-1 and RBP-2; *P. reichenowi* RH5; and *P. yoelii* Py01365), N-terminal PfRH5-like domains were identified with high confidence, despite sequence identities of 14-22% and a lack of totally conserved residues or disulphide bonds (Extended Data Fig. 4a). Similar residues are located primarily in the interior of the domain, where they may stabilise the fold (Extended Data Fig. 4b). In PfRH4, the only other RH protein with a known erythrocyte receptor, the complement receptor 1 (CR1) binding fragment contains the putative PfRH5 fold[14]. These PfRH5-like domains are therefore excellent candidates for ligand-binding modules in other RH proteins.

Basigin binds at the tip of PfRH5, distant from the flexible loop and C-terminus, with both domains and the intervening linker directly contacting PfRH5 (Fig. 2A,D). Most of the contact area (~1350 $Å^2$) occurs through hydrogen bonds between the backbone of strands A and G of the basigin N-terminal domain and loops at the tip of PfRH5 (Extended Data Table 2a). PfRH5 residues F350 and W447 stabilise this interaction by packing into hydrophobic pockets on basigin. The limited involvement of basigin side chains will reduce the potential for basigin escape mutants that prevent PfRH5 binding and impair parasite invasion.

The basigin C-terminal domain and H102 in the linker also directly contact PfRH5 (Extended Data Table 2a). The three loops at the tip of the basigin C-terminal domain (linking strands B and C, strands D and E and strands F and G) interact with the second and fourth helices of PfRH5 through hydrogen bonds and a hydrophobic patch contributed by residues VPP from the BC loop. However, flexibility of the basigin linker allows different orientations of the C-terminal domains in the two copies in the asymmetric unit of the crystal. Chain B interacts through the BC and DE loops (a ~650 $Å^2$ interface) while chain D interacts through the BC and FG loops (~480 $Å^2$) (Fig. 2b), leading to a maximum difference of ~18Å in the position of the C-terminus in the two complexes. Flexibility is also predicted from SAXS analysis of the complex in solution (Extended Data Fig. 3). While

PfRH5 and the basigin N-terminal domain fit the SAXS envelope, the C-terminal domain only partially fits, consistent with a flexible interaction with PfRH5.

PfRH5 is highly conserved, with just twelve non-synonymous SNPs in 227 field isolates, and only five at frequencies of 10% or greater[7,8,12]. These SNPs are distributed across the structure but do not affect residues that directly contact basigin (Extended Data Fig. 5). By contrast, in sequenced laboratory strains, eight PfRH5 SNPs are associated with increased ability to invade *Aotus* erythrocytes[15,16]. A number of these (I204, N347, Y358 and E362) are in or close to the basigin binding site, and may affect host tropism. Basigin residues which, when mutated, affect PfRH5 affinity (F27, Q100 and H102)[17] are also located at the interface.

The two PfRH5:basigin complexes in the asymmetric unit pack together through basigin-mediated contacts, including a ~911 $Å^2$ interface between the two basigin C-terminal domains, bringing their C-termini into close proximity (Extended Data Fig. 6). As yet, the role of PfRH5 in invasion is uncertain, but it is tempting to speculate that this 2:2 complex assembles during invasion, mediating a signalling event in either parasite or erythrocyte to trigger an essential downstream process. This would leave one face of PfRH5 available for binding of PfRipr[10] and other, as yet unidentified, binding partners. However, in solution (at concentrations ≤24 μM) we observe no 2:2 complex, either through SAXS (Extended Data Fig. 3) or analytical ultracentrifugation (Fig. 2C, Extended Data Fig 7). Whether such a complex assembles at high local concentrations during invasion remains to be elucidated.

To identify inhibitory epitopes, complexes of PfRH5ΔNL with Fab fragments from three inhibitory monoclonal antibodies were studied by crystallography and SAXS. QA1 and QA5 were previously shown to block PfRH5-basigin binding and parasite growth. 9AD4 does not block PfRH5-basigin binding *in vitro*, but is one of the most effective antibodies currently available for inhibiting parasite growth[5]. Crystal structures of PfRH5 bound to QA1 and 9AD4 were confirmed by SAXS, while a model for PfRH5:QA5 was derived from SAXS analysis, guided by a previously identified linear epitope (residues 201-213 from helix 2)[5].

The antibodies bind to three distinct sites, close to the vertex of PfRH5 (Fig. 3, Extended Data Fig. 8, Extended Data Table 2b,c). QA1 binds to loops at the PfRH5 tip, overlapping the basigin N-terminal domain binding site. QA5 predominantly interacts with PfRH5 helix 2, overlapping the basigin C-terminal domain binding site. In contrast, 9AD4 binds helices 2 and 3, close to, but not overlapping, either basigin binding site. This is likely to allow intact 9AD4 IgG to impede erythrocyte binding when PfRH5 and basigin are both membrane-tethered. This reveals inhibitory epitopes in, or close to, the basigin binding sites, that can be targeted to block parasite invasion.

In summary, PfRH5 adopts a novel architecture, formed, as in many families of parasite surface proteins[18], from a robust α-helical scaffold. This maintains the overall fold by retaining residues required for helical packing, while allowing significant surface sequence variation. Sequence homology identifies this fold at the N-terminus of other RH proteins, where it is likely to act as a ligand-binding module.

Characterisation of the PfRH5:basigin complex prompts a range of future experiments to investigate the role of PfRH5 in erythrocyte invasion. Furthermore, monoclonal antibodies that block parasite growth bind at or close to the basigin-binding site. Immunogens containing these regions of PfRH5 will be important components of a vaccine to prevent *P. falciparum* erythrocyte invasion, thereby crippling the parasite responsible for the deadliest form of human malaria.

Methods

Basigin cloning, expression and purification

A section of the basigin gene encoding immunoglobin domains 1 and 2 of the short isoform (residues 22-205) was amplified from cDNA using primers: 5′-CCGGATCCGCTGCCGGAACCGTGTTC-3′ and CCCATATGCTAGTGTGACCGCACTCTCAGG-3′. PCR products were cloned into a modified pET15b vector (Novagen), which encodes an N-terminal hexa-histidine tag followed by a tobacco etch virus (TEV) protease cleavage site. TEV cleavage leaves an additional glycine at the N-terminus from the cleavage site.

Basigin was expressed in bacterial strain Origami B (DE3) (Novagen) by incubation overnight at 25°C after induction with 1mM IPTG. The protein was purified by nickel-nitrilotriacetic acid (Ni^{2+}-NTA; Qiagen) affinity chromatography, followed by buffer exchange into PBS using a PD-10 desalting column (GE Healthcare), and overnight cleavage with His-tagged TEV protease at 4°C, before a second Ni^{2+}-NTA column. The flow-through was concentrated using an Amicon Ultra centrifugal filter device (molecular mass cutoff, 3,000 Da). Finally, gel filtration was performed with a Superdex 200 16/60 column (GE Healthcare) in 20 mM HEPES (pH 7.5) and 150 mM NaCl.

Expression and purification of 9AD4, QA1 and QA5

Anti-PfRH5 monoclonal antibodies were described previously[5]. Hybridomas expressing 9AD4, QA1 and QA5 were grown in Dulbecco's Modified Eagle's Medium (DMEM; Sigma) supplemented with 4 mM L-glutamine (Sigma), 0.01 M HEPES (Life Technologies), 100 U penicillin and 0.1 mg/ml streptomycin (Sigma), and 20% fetal calf serum (Gibco). They were then transferred into CD Hybridoma medium (Life Technologies) with glutamine, penicillin, and streptomycin. The cells were harvested after 7-10 days. The cell culture supernatant was exchanged into 20 mM phosphate pH 7.0 with a tangential flow filtration device (Pall).

The sample was then loaded onto a HiTrap Protein G HP column (GE Healthcare), eluted in 0.1 M glycine-HCl (pH 3.0), and immediately neutralised with 0.1 M Tris (pH 8.0). The sample was exchanged into 100 mM phosphate (pH 6.4), 300 mM NaCl, 2 mM EDTA, 5 mM L-cysteine (pH 6.4), and 1.5 mM β-mercaptoethanol using PD-10 columns (GE Healthcare).

Antibody fragments were generated by addition of papain agarose (Sigma), and overnight incubation at 37°C. The papain agarose was removed by centrifugation, and the sample loaded onto a HiTrap Protein A HP column (GE Healthcare). The material that did not bind

to the column was gel filtered on a Superdex 200 16/60 column (GE Healthcare) in 20 mM HEPES (pH 7.5) and 150 mM NaCl.

PfRH5 cloning, expression and purification

A synthetic gene was designed encoding full-length PfRH5 residues E26-Q526 from *Plasmodium falciparum* strain 7G8, codon optimised for expression in *Drosophila melanogaster*, with four putative glycosylation sites removed by mutation of asparagines to alanines (Life Technologies). The gene was flanked by an EcoRI site and Kozak sequence at the 5′ end, and a NotI site at the 3′ end. Long-range disorder was predicted using POODLE-L[19]. A shortened mutant, PfRH5ΔN, lacking the flexible N-terminus, was also synthesised, encompassing residues K140-Q526. A further mutant, PfRH5ΔNL, was generated by removal of a predicted disordered loop (residues N248-M296) in addition to the N-terminal truncation. All constructs contained a C-terminal hexa-histidine tag. PfRH5 constructs were subcloned into pExpreS^2-1 (ExpreS^{2}ion Biotechnologies, Horsholm, Denmark).

Constructs were transfected into Schneider 2 (S2) cells using ExpreS^2 Insect-TRx5 (ExpreS^{2}ion) transfection reagent, and a polyclonal cell line was selected over three weeks in EX-CELL 420 insect cell media with L-glutamine (Sigma) supplemented with 10% fetal calf serum (Gibco) and 1.5 mg/ml zeocin. The stable cell lines were then expanded in EX-CELL 420 media without fetal calf serum or zeocin. Four days after the final split, the cells were harvested, and the cell culture supernatant exchanged into 20 mM phosphate, pH 7.4, 250 mM NaCl, 20 mM imidazole, and 0.005% Tween-20, using a tangential flow filtration device (Pall). Protein purification from the supernatant then proceeded through Ni^{2+}-NTA (HisTrap FF; GE Healthcare) and ConA lectin-binding chromatography (HiTrap ConA 4B; GE Healthcare).

Full-length PfRH5, PfRH5ΔN and PfRH5ΔNL for biophysical analysis were subjected to gel filtration on a Superdex 200 16/60 column (GE Healthcare), and concentrated with an Amicon centrifugal filter device (molecular weight cut-off, 10,000 Da).

To prepare PfRH5ΔNL for crystallisation, the sample was cleaved overnight with endoproteinase GluC (Sigma) at 20°C. At this point, basigin, 9AD4, or QA1 was added to the protein. To methylate the complex, 0.02 M dimethylamine-borane complex (ABC) and 0.04 M formaldehyde were added and the reaction incubated at 4°C for 1 hour. An additional 0.02 M ABC and 0.04 M formaldehyde were added; after another 1 hour, 0.01 M ABC was added and the reaction was incubated at 4°C overnight. Finally, the complexes were gel filtered and concentrated as detailed above.

Surface plasmon resonance

Surface plasmon resonance experiments were carried out using a BIAcore T200 instrument (GE Healthcare). Experiments were performed at 20°C in 10 mM HEPES (pH 7.4), 150 mM NaCl, 3 mM EDTA, 0.005% Tween 20, 2 mg/ml dextran, and 1 mg/ml salmon sperm DNA (Sigma Aldrich). Basigin was immobilized on a CM5 chip (GE Healthcare) by amine coupling (GE Healthcare kit) to a total of 850 RU. A concentration series of PfRH5ΔNL (8, 4, 2, 1, 0.5, 0.25, 0.125, and 0.0625 μM) was injected over the basigin-coated chip for 120 s

at 30 μl/min, followed by a 300 s dissociation time. The chip surface was then regenerated with 30 s of 2 M NaCl. Specific binding of PfRH5ΔNL was obtained by subtracting the response from a blank surface from that of the basigin-coated surface. The kinetic sensorgrams were fitted to a global 1:1 interaction model, allowing determination of the dissociation constant, K_d, using BIAevaluation software 1.0 (GE Healthcare).

Assays of growth inhibition activity (GIA)

Rabbit immunisations were carried out by Biogenes (Germany). Female ZiKa rabbits (n=4) were immunised intramuscularly (i.m.) with 20μg PfRH5ΔNL protein formulated in complete Freund's adjuvant on day 0, followed by two booster immunisations i.m. on days 28 and 56 with the same dose of protein formulated in incomplete Freund's adjuvant. Control rabbits received the same immunisation schedule with 50μg ovalbumin protein. Sera were collected two weeks after the final immunisation and shipped frozen.

Total IgG was purified from rabbit sera using protein G columns (Pierce). The *P. falciparum* 3D7 and 7G8 lines were maintained in continuous culture using fresh O^+ erythrocytes at 2% haematocrit and synchronised by two incubations in 5% sorbitol 6-8 h apart. Synchronised trophozoites were adjusted to 0.3% parasitaemia and then incubated for 42 h with the various IgG concentrations (tested in triplicate). Final parasitaemia was determined by biochemical determination of parasite lactate dehydrogenase[20]. Percentage growth inhibition is expressed relative to wells containing IgG from control immunised rabbits[6]. The mean of the three replicate wells was taken to obtain the final data for each individual rabbit at each tested IgG concentration. Experiments were performed twice against each strain of parasite with very similar results. A representative experiment is shown in Fig. 1D. The mean ± standard error of mean are plotted for the results obtained with the purified IgG from the four immunised rabbits.

ELISA

Maxisorp plates were coated with anti-PfRH5 mouse monoclonal antibody[5] (50μL/well at 5μg/mL) and left at 4°C overnight. Following six washes in PBS with 0.05% Tween-20 (PBS-T), plates were blocked with 150 μL/well Casein block solution (Pierce) for 1 h, followed by another six PBS-T washes. PfRH5ΔNL protein was added to wells in triplicate (50 μL/well) at four dilutions in blocking buffer (800, 200, 50 and 12.5 ng/mL) and incubated at room temperature for 2 h. Following another six PBS-T washes, plates were incubated with polyclonal anti-full-length PfRH5 rabbit serum[6] diluted 1:1000 in blocking solution, 50 μL/well for 1 h. Following another PBS-T wash, plates were incubated with goat anti-rabbit IgG alkaline phosphatase diluted 1:5000 in blocking solution, 50 μL/well for 1 h. Following a final six PBS-T washes, and two PBS washes, plates were developed and optical density read at 405nm as previously described[21].

Crystallisation, data collection and data processing of PfRH5 complexes

Crystallisation was achieved using vapour diffusion in sitting drops. A TTP Labtech Mosquito LCP robot was employed to mix 100 nl of each protein complex at 8 mg/ml with 100 nl of well solutions from commercially available crystal screens. Crystals were first obtained in conditions from the Proplex (RH5ΔNL:basigin), JCSG+ (RH5ΔNL:9AD4) and

Morpheus (RH5ΔNL:QA1) crystal screens (Molecular Dimensions). The well solution for PfRH5ΔNL:basigin was 0.2 M lithium sulphate, 0.1 M MES (pH 6.0), and 20% (w/v) PEG 4000. For PfRH5ΔNL:9AD4, the well solution was 24% (w/v) PEG 1500 and 20% (v/v) glycerol. PfRH5ΔNL:QA1 was crystallised in a 0.12 M mix of 1,6-hexanediol, 1-butanol, 1,2-propanediol, 2-propanol, 1,4-butanediol, 1,3-propanediol; 0.1 M MES-imidazole (pH 6.5); 20% (w/v) PEG 550 MME; and 10% (w/v) PEG 20,000. Crystals were obtained at 4°C for PfRH5ΔNL:basigin and PfRH5ΔNL:9AD4, and at 18°C for PfRH5ΔNL:QA1. Crystal seeds were generated by adding crystals in well solution to a Seed Bead (Hampton Research) and vortexing for 15 seconds. New crystal drops were then set up by mixing 100 nl of 8 mg/ml protein complex, 50 nl of well solution, 50 nl of seeds, and 50 nl of Silver Bullets or Silver Bullets Bio additives (Hampton Research). RH5ΔNL:basigin crystals were cryoprotected by transfer into well solution supplemented with 25% ethylene glycol, then cryocooled by plunging into nitrogen. PfRH5ΔNL:9AD4 crystals were directly cryocooled. PfRH5ΔNL:QA1 crystals were cryoprotected in well solution with a total of 32% (w/v) PEG 550 MME and 16% (w/v) PEG 20,000 before cryocooling.

Data were collected at the Diamond Light Source, on beamline I04-1 for the PfRH5ΔNL:basigin complex (wavelength 0.92 Å), and on beamline I04 for both PfRH5ΔNL:Fab complexes (wavelength 0.97949 Å). Data reduction was performed using iMosflm[22,23] and scala[24] from the CCP4 processing suite[25]. A composite of the light chain from PDB entry 3QQ9 and the heavy chain from 3HR5 was used as a molecular replacement model for 9AD4 in Phaser[26]. Density modification was performed with PARROT[27]. Buccaneer[28] was employed to build helices into initial PfRH5ΔNL density, initiating a cycle of model building and refinement using REFMAC[29], BUSTER[30], and Coot[31]. PfRH5ΔNL was used as a molecular replacement model in Phaser[26], together with basigin (PDB code 3B5H) for the PfRH5ΔNL:basigin structure, or with a composite of the heavy chain from 2ZN9 and the light chain from 1I7Z for the PfRH5ΔNL:QA1 structure. Refinement was accomplished with BUSTER[30]. Ramachandran statistics, determined using PROCHECK[32], were as follows: for PfRH5ΔNL:basigin, 93% of residues fell in the allowed regions and 7% in the additional allowed region; for PfRH5ΔNL:9AD4, 93.9% were in the allowed region, 5.8% were in the additional allowed region, and 0.2% were in the generously allowed region; and for PfRH5ΔNL:QA1, 86.0% were in the allowed region, 13.3% were in the additional allowed region, and 0.7% were in the generously allowed region. There were no residues in the disallowed region of the Ramachandran plot in any of the structures.

Alignment of RH protein sequences

Sequences of *P. falciparum* RH1, RH4, RH2a, RH2b, and RH3; *P. vivax* RBP-1 and RBP-2; *P. reichenowi* RH5; and *P. yoelii* Py01365 were aligned against PfRH5 using the Clustal Omega server[33], and an alignment figure generated with ESPript[34]. The homologous portion of each sequence was then threaded onto the PfRH5 structure using the Phyre2 server[35].

Europe PMC Funders Author Manuscripts

Small-angle X-ray scattering data collection and processing

Small-angle X-ray scattering (SAXS) data were collected at beamline BM29 at the European Synchrotron Radiation Facility (ESRF, Grenoble, France). Scattering was detected using a Pilatus image reader at 20°C.

Full-length PfRH5:basigin, PfRH5:QA1 and PfRH5:QA5 complexes were prepared by mixing the individual proteins in equimolar amounts, and gel filtering on a Superdex 200 16/60 column in 20 mM HEPES (pH 7.5), 150 mM NaCl. PfRH5:9AD4 samples were prepared by mixing PfRH5 and 9AD4 in equimolar amounts for 10 minutes. 60 μl samples were prepared in serial dilutions between 0.2-2.0 mg/ml.

Ten consecutive frames of 10 s each were recorded for each protein sample, with buffer samples measured in between. The frames were inspected for any evidence of radiation damage, and any affected images were excluded from further processing. Data were normalised to the intensity of the incident beam, images were averaged, and buffer scattering subtracted using PRIMUS[36,37]. Guinier plots were inspected to assess the presence of aggregation[38]. Composite curves were generated by scaling and merging appropriate data sets. The radius of gyration (R_g) was determined from the Guinier plot using AutoRg[37]. The distance distribution function (P(r)) was obtained by indirect Fourier transform, generating an estimate of the maximum particle dimension (D_{max}) and the Porod volume of the hydrated particle[37,39]. An estimate of the molecular weight was obtained by dividing the Porod volume by 1.7. Twenty *ab initio* shape reconstructions were generated with DAMMIF[40] and averaged with DAMAVER[41]. The normalized spatial discrepancy (NSD) parameter was used to diagnose the similarity of the reconstructions[42]. SITUS and SCULPTOR[43] were used to dock atomic structures into the SAXS envelopes.

Analytical ultracentrifugation

Analytical ultracentrifugation experiments were carried out using a Beckman An-60 Ti rotor in a Beckman Optima XL-1 analytical ultracentrifuge at 20°C. Samples were prepared at concentrations of 0.5-1.0 mg/ml in 20 mM HEPES (pH 7.5), and 150 mM NaCl.

The samples for sedimentation velocity experiments were full-length PfRH5, basigin, and a PfRH5:basigin complex prepared by gel filtration. Scans were recorded using interference optics. Multiple scans were fit to a continuous size distribution using SEDFIT[44,45]. The buffer density and viscosity were calculated with SEDNTERP[46]. The sample partial specific volumes were estimated from the amino acid sequences, also using SEDNTERP.

During the time course of a sedimentation equilibrium experiment, degradation of full-length PfRH5 was observed. Therefore experiments were performed using PfRH5ΔN. Basigin, PfRH5ΔN and a gel filtered PfRH5ΔN:basigin complex were analysed at 22 μM, 9 μM, and 9 μM, respectively. The run proceeded for 20 hours at different speeds and scans recorded the UV absorbance at 280 nm. The buffer density and viscosity, together with sample partial specific volumes, were calculated as above[46]. The data were fit to an ideal monodisperse model using SEDPHAT[47], with the assumption that at concentrations of ~10 times the K_D, PfRH5ΔN is fully complexed with basigin.

Europe PMC Funders Author Manuscripts

Extended Data

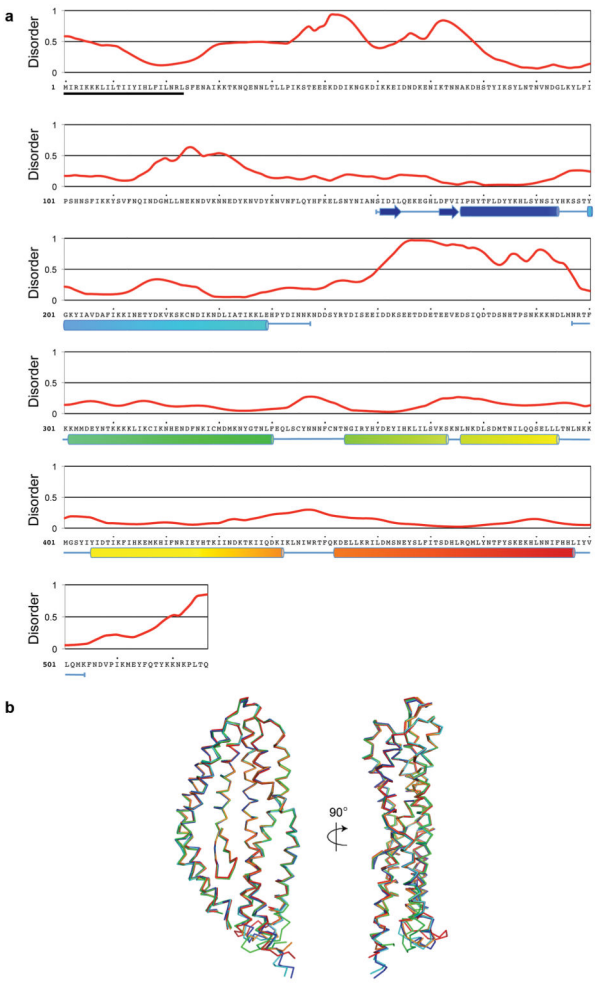

Extended Data Figure 1. PfRH5 disorder predictions and structural alignment

a, Long-range disorder was predicted by POODLE-L[19] and was used to determine domain boundaries for the PfRH5ΔNL crystallisation construct. The disorder predictions are shown above the sequence of PfRH5, with values of >0.5 indicative of disorder. The residues visible in the PfRH5ΔNL crystal structure are shown below the PfRH5 sequence as secondary structure elements (sheets as blue arrows, and helices as tubes in rainbow coloring) linked by blue lines. The missing loop (248-296) is shown as a break in the blue line. The secretion signal sequence is indicated (black underline). **b,** Two copies of PfRH5 from the PfRH5:basigin structure (red and orange), two copies from the PfRH5:QA1 structure (blue and cyan), and one copy from PfRH5:9AD4 (green) structure were aligned using Coot[31], giving an RMSD of 1.7 Å. The C-terminus and the loop between helices 4 and 5 were the only regions showing significant differences. For the remaining 95% of PfRH5, the RMSD is 0.9 Å.

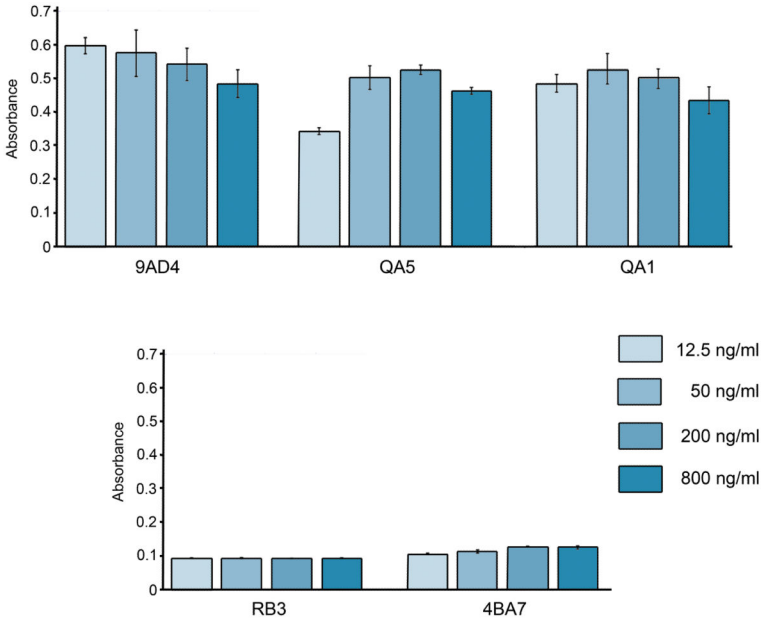

Extended Data Figure 2. Investigation of the interaction of PfRH5ΔNL with a panel of mouse mAbs using ELISA

Five mAbs that bind to PfRH5 were coated on a ELISA plate and probed using PfRH5ΔNL at concentrations of 12.5, 50, 200 or 800 ng/ml. Antibodies 9AD5, QA1 and QA5 interacted with PfRH5ΔNL while RB3 and 4BA7 did not. Indeed, RB3 and 4BA7 bind to the flexible N-terminus and the truncated loop, respectively, both features lacking in PfRH5ΔNL[5]. The error bars are standard error of mean (n=3).

Europe PMC Funders Author Manuscripts

Europe PMC Funders Author Manuscripts

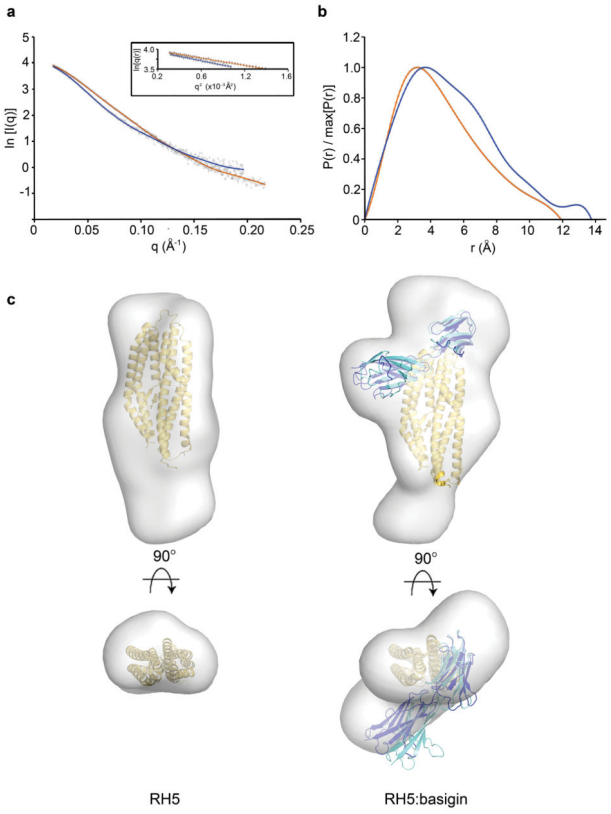

d

	Rg (*nm*)	Dmax (*nm*)	Porod volume (nm^3)	MW_{app} (*kDa*)	NSD	χ
PfRH5	3.7	11.9	104.5	61.4	0.692±0.036	1.01
PfRH5: basigin	4.1	13.8	138.3	81.3	0.715±0.034	0.74

Extended Data Figure 3. SAXS analysis of the PfRH5:basigin complex

a, The theoretical scattering calculated from the average of 20 *ab initio* reconstructions (continuous lines, with PfRH5 in orange and PfRH5:basigin in blue) plotted with the experimental scattering intensity curves (diamonds). The data are presented as the natural logarithm of the intensity. Guinier plots are displayed in the inset. **b**, The distance distribution function, P(r), of PfRH5 (orange) and PfRH5:basigin (blue). **c**, To the left, the crystal structure of PfRH5ΔNL (yellow) was docked into the average *ab initio* SAXS envelope of full-length PfRH5 (grey). Extra density corresponding to some or all of the truncated regions is visible at the bottom of the kite-like structure, near the C-terminus. To the right, the crystal structure of PfRH5ΔNL:basigin is docked into the average *ab initio* SAXS envelope of full-length PfRH5:basigin (grey). PfRH5ΔNL is yellow. In dark blue and cyan are basigin molecules from the two PfRH5ΔNL:basigin complexes in the asymmetric unit, superimposed based on the structure of PfRH5ΔNL. **d**, Summary of SAXS parameters. The radius of gyration (R_g) was determined from the Guinier plot using AutoRg[37], and the maximum particle dimension (Dmax) and the Porod volume[39] were calculated using GNOM[37]. An estimate of the molecular weight was obtained by dividing the Porod volume by 1.7. *Ab initio* modeling was used to generate 20 shape reconstructions from the data. The

normalised spatial discrepancy parameter (NSD) diagnoses the similarity of these models[42]. The models were averaged and the fit of the average model to the experimental data is indicated by the χ value.

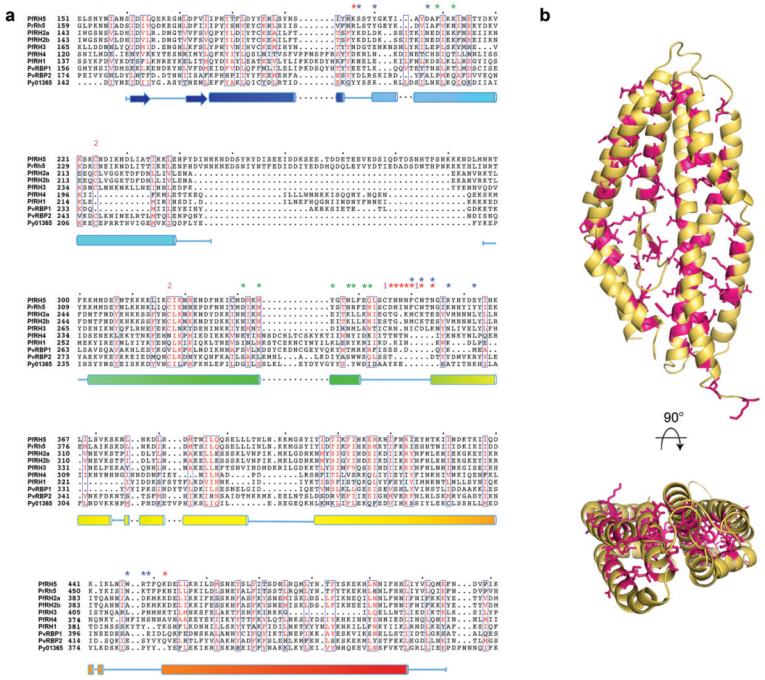

Extended Data Figure 4. A conserved PfRH5-like fold in other *Plasmodium* RH proteins

a, *P. falciparum* RH1, RH4, RH2b, RH2a and RH3 (a pseudogene); *P. vivax* RBP-1 and RBP-2; *P. reichenowi* RH5; and *P. yoelii* Py01365 were aligned using Clustal Omega[33] and were threaded using the Phyre2 server[35], giving more than 98% confidence of fold conservation over >260 residues in each case. The secondary structure of PfRH5 is shown below the sequence in a rainbow colour scheme as in Fig. 1A. Residues from PfRH5 that interact with basigin, QA1 and 9AD4 are indicated above the sequence by blue, red or green stars respectively. Cysteine residues that make disulphide bonds are indicated by pink numbers, with residues sharing the same number forming a disulphide bond. **b,** PfRH5 is shown in yellow, with residues similar among RH proteins (from the alignment in extended data figure 4) highlighted as pink sticks. The majority of the similar residues appear to play a structural role stabilising the architecture of the domain.

Europe PMC Funders Author Manuscripts

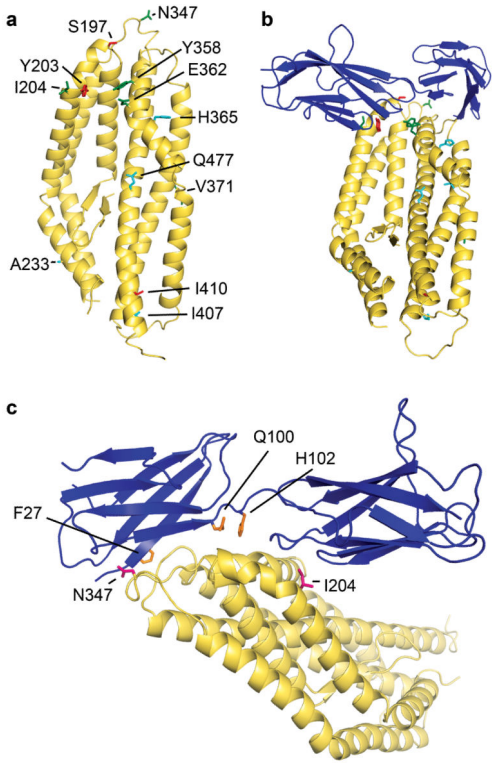

Extended Data Figure 5. Location of PfRH5 polymorphisms, and residues of PfRH5 and basigin implicated in host tropism

a and **b**, Indicated are the locations of PfRH5 SNPs that are common (10% frequency or greater; red sticks) or uncommon (blue sticks) among 227 field isolates[7,8,12], as well as additional SNPs observed in lab strains (green sticks)[15,16]. **b**, Basigin (blue) is shown in addition to PfRH5 (yellow). SNPs Y203, I204, N347, Y358, and E362 are localized in or near the PfRH5:basigin interface. Not visible in this orientation is lab strain polymorphism K429. **c**, Highlighted are basigin residues F27, Q100, and H102, which affect the affinity for PfRH5 when mutated[17] (orange sticks). Also shown are two SNPs of PfRH5, namely N347 and I204 (pink sticks), found in the PfRH5:basigin binding interface and linked to the strain's ability to invade *Aotus* monkey erythrocytes[15].

Europe PMC Funders Author Manuscripts

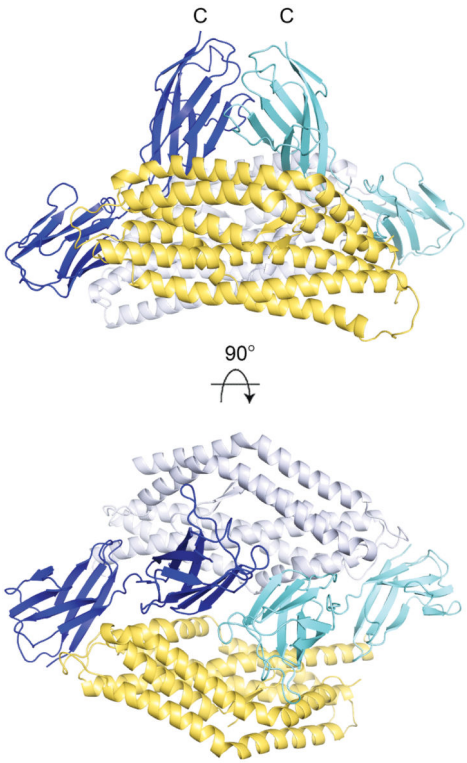

Extended Data Figure 6. Arrangement of two PfRH5:basigin complexes in the asymmetric unit of the crystal

One complex, shown in yellow (PfRH5) and blue (basigin), interacts with the second, shown in silver (PfRH5) and cyan (basigin), primarily through packing between the two C-terminal domains of basigin. The two C-termini of basigin are in close proximity (top view).

Europe PMC Funders Author Manuscripts

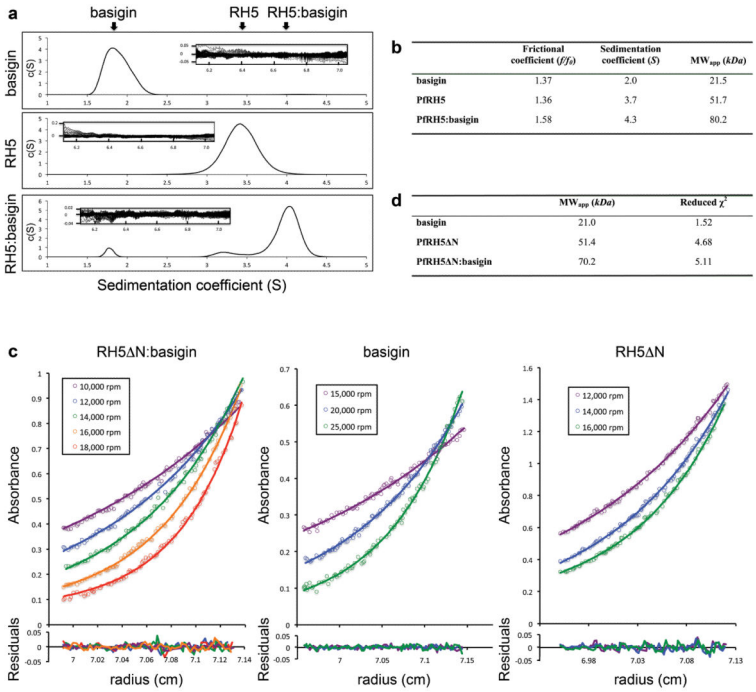

Extended Data Figure 7. Analysis of the PfRH5:basigin complex using analytical ultracentrifugation

a-b, Sedimentation velocity analysis. The continuous sedimentation coefficient distributions that best fit the data are shown for basigin (top), full-length PfRH5 (middle), and a gel filtered PfRH5:basigin complex (bottom). The inset shows the fitting residuals. **c-d,** Sedimentation equilibrium analysis. PfRH5ΔN (residues 140-526), basigin, and a gel filtered PfRH5ΔN:basigin complex were analysed. The runs lasted 20 hours at different speeds, as indicated in the inset legends. UV absorbance was monitored at 280 nm. The residuals are shown below fitted data. The calculated molecular weights are consistent with the formation of a 1:1 complex between PfRH5ΔN and basigin.

Europe PMC Funders Author Manuscripts

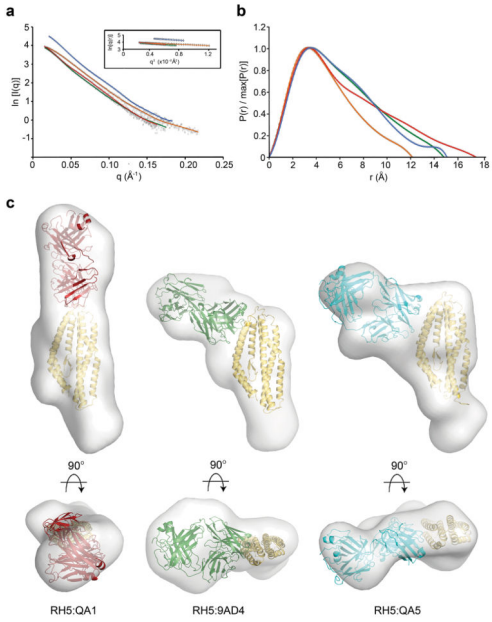

d

	Rg (*nm*)	Dmax (*nm*)	Porod volume (nm^3)	MW_{app} (*kDa*)	NSD	χ
PfRH5	3.7	11.9	104.5	61.4	0.692±0.036	1.01
PfRH5: 9AD4	4.6	14.6	154.5	90.9	0.759±0.55	0.95
PfRH5: QA1	4.9	17.2	152.4	89.6	0.789±0.032	0.97
PfRH5: Qa5	4.4	14.8	157.9	92.9	0.643±0.023	0.89

Extended Data Figure 8. SAXS of PfRH5 in complex with growth-inhibitory Fab fragments

a, The theoretical scattering calculated from the average of 20 *ab initio* reconstructions (continuous lines, with PfRH5 in orange, PfRH5:9AD4 in green, PfRH5:QA1 in red, and PfRH5:QA5 in blue) plotted with the experimental scattering intensity curves (black diamonds). The data are presented as the natural logarithm of the intensity. The Guiner plots are displayed in the inset. **b**, The distance distribution function, P(r), with colours as in **a**. **c**, The crystal structures of PfRH5ΔNL:QA1(left) and PfRH5ΔNL:9AD4 (middle) were docked into the corresponding full-length PfRH5:Fab envelopes (grey). PfRH5ΔNL is shown in yellow, QA1 in red, and 9AD4 in green. PfRH5ΔNL and a Fab fragment (cyan) were docked into the PfRH5:QA5 SAXS envelope to generate a model of the PfRH5:QA5 structure (right). **d,** A summary of SAXS parameters. The radius of gyration (R_g) was determined from the Guinier plot using AutoRg[37], and the maximum particle dimension (Dmax) and the Porod volume[39] were calculated using GNOM[37]. An estimate of the molecular weight was obtained by dividing the Porod volume by 1.7. *Ab initio* modeling was used to generate 20 shape reconstructions from the data. The normalised spatial discrepancy parameter (NSD) diagnoses the similarity of these models[42]. The models were averaged and the fit of the average model to the experimental data is indicated by the χ value.

Europe PMC Funders Author Manuscripts

Europe PMC Funders Author Manuscripts

Extended Data Table 1

Crystallographic data collection and refinement statistics

	PfRH5ΔNL:basigin	PfRH5ΔNL:9AD4	PfRH5ΔNL:QAl
Data collection			
Space group	$P2_12_12_1$	$P2_12_12_1$	$P22_12_1$
Cell dimensions			
a, *b*, *c* (Å)	75.28, 109.36, 151.95	39.79, 86.66, 324.04	65.12, 137.30, 228.58
α,*β*,*γ*(°)	90.00, 90.00, 90.00	90.00, 90.00, 90.00	90.00, 90.00, 90.00
Resolution (Å)	67.46 – 3.10(3.27-3.10)	41.86-2.30 (2.42-2.30)	47.24-3.10(3.27-3.10)
R_{pim}	0.080 (0.297)	0.047 (0.375)	0.049 (0.380)
$I/\sigma I$	9.4 (2.7)	9.8 (2.0)	9.2 (2.3)
Completeness (%)	99.8 (99.8)	96.2 (83.3)	95.5 (96.3)
Redundancy	6.1 (6.2)	5.0 (4.4)	4.5 (4.6)
Refinement			
Resolution (Å)	67.46-3.10	41.86-2.30	47.24-3.10
No. reflections	23357	49336	36259
R_{work}/ R_{free} (%)	21.71 / 24.45	22.10 / 25.83	23.6 / 28.1
No. atoms	7629	6005	11478
Wilson B-factors	48.0	41.1	90.1
R.m.s deviations			
Bond lengths (Å)	0.010	0.014	0.013
Bond angles (°)	1.5	1.7	1.9

Extended Data Table 2

Description of interactions between PfRH5 with basigin or monoclonal antibodies QA1 and 9AD4

a

PfRH5			Basigin			
Chain	**Residue**	**Group**	**Chain**	**Residue**	**Group**	**Interaction**
			N-terminal domain:			
A/C	S197	side chain	B/D	Q100	side chain NH2	hydrogen bond
A/C	S197	side chain	B/D	E84	side chain	hydrogen bond
A/C	F350	side chain	B/D		hydrophobic	hydrophobic
A/C	N352	side chain CO	B/D	N98	backbone NH	hydrogen bond
A/C	N354	side chain NH2	B/D	N98	backbone CO	hydrogen bond
A/C	R357	side chain	B/D	V26	backbone CO	hydrogen bond

a

PfRH5			Basigin			
Chain	**Residue**	**Group**	**Chain**	**Residue**	**Group**	**Interaction**
A/C	W447	side chain	B/D		hydrophobic	hydrophobic
A/C	W447	backbone CO	B/D	T28	backbone NH	hydrogen bond
A/C	R448	side chain	B/D	T25	side chain	hydrogen bond
A/C	T449	side chain	B/D	V26	backbone NH	hydrogen bond
A/C	T449	backbone NH	B/D	V26	backbone CO	hydrogen bond
			Linker:			
A/C	Y200	side chain	B/D	H102	side chain	hydrogen bond
			C-terminal domain:			
A/C		hydrophobic	B/D	V131	side chain	hydrophobic
A		hydrophobic	B	P133	side chain	hydrophobic
A	D207	side chain	B	Q164	side chain NH2	hydrogen bond
C	E362	side chain	D	K191	side chain	hydrogen bond
C	E362	side chain	D	S190	side chain	hydrogen bond

b

PfRH5			QA1			
Chain	**Residue**	**Group**	**Chain**	**Residue**	**Group**	**Interaction**
			Heavy chain:			
A/D	K196	side chain	B/E	N101	side chain CO	hydrogen bond
A/D	K196	side chain	B/E	D31	backbone CO	hydrogen bond
A/D	S197	backbone NH	B/E	D53	side chain	hydrogen bond
A/D	Y346	side chain	B/E	Y33	side chain	pi stacking
A/D	N348	side chain CO	B/E	G105	backbone NH	hydrogen bond
A/D	N352	side chain	B/E	Y33	side chain	hydrogen bond
A/D	N352	side chain	B/E	Y59	side chain	hydrogen bond
A/D	N354	backbone NH	B/E	Y57	side chain	hydrogen bond
A/D	K452	side chain	B/E	D104	side chain	hydrogen bond
			Light chain:			
A/D	N347	side chain NH2	C/F	S95	backbone CO	hydrogen bond

b

PfRH5			QA1			
Chain	**Residue**	**Group**	**Chain**	**Residue**	**Group**	**Interaction**
A/D	N348	backbone NH	C/F	Y36	side chain	hydrogen bond
A/D	N349	backbone NH	C/F	Y34	side chain	hydrogen bond
A/D	N349	side chain CO	C/F	W96	side chain	hydrogen bond
A/D	F350	side chain	C/F		hydrophobic	hydrophobic
A/D	Q451	backbone CO	C/F	Y34	side chain	hydrogen bond

c

PfRH5			9AD4			
Chain	**Residue**	**Group**	**Chain**	**Residue**	**Group**	**Interaction**
			Heavy chain:			
A	A205	backbone CO	B	Y103	backbone CO	hydrogen bond (H_20)
A	F209	side chain	B		hydrophobic	hydrophobic
A	Y335	side chain	B	Y103	backbone CO	hydrogen bond
A	N338	side chain CO	B	W107	side chain	hydrogen bond
A	L339	side chain	B		hydrophobic	hydrophobic
A	E341	side chain	B	S52	side chain	hydrogen bond
A	E341	side chain	B	M54	backbone CO	hydrogen bond
A	E341	side chain	B	A55	backbone CO	hydrogen bond
A	E341	side chain	B	Y56	backbone CO	hydrogen bond
A	Q342	side chain CO	B	N53	side chain NH2	hydrogen bond
A		hydrophobic	B	F101	side chain	hydrophobic
			Light chain:			
A	K212	side chain	C	Y32	backbone CO	hydrogen bond
A	D331	side chain	C	Y32	side chain	hydrogen bond
A	N334	side chain NH2	C	Y31	side chain	hydrogen bond (H_20)

Acknowledgments

MKH is a Wellcome Trust Investigator (101020/Z/13/Z). KEW is funded by a Wellcome Trust Ph.D. studentship. SJD holds a UK Medical Research Council (MRC) Career Development Fellowship (G1000527), is a Jenner Investigator and Lister Institute Research Prize Fellow. The project was also funded by the European Vaccine Initiative (EVI) (InnoMalVac); the UK MRC (MR/K025554/1), the European Community's Seventh Framework

Programme (FP7/2007-2013, grant agreement number 242095 – EVIMalaR); a Wellcome Trust Training Fellowship (089455/2/09/z to ADD). We thank Julie Furze and Daniel Alanine (Jenner Institute); David Staunton and Edward Lowe (Department of Biochemistry, Oxford University); Adam Round (ESRF); and Ralf Flaig and Jose Brandao-Neto (Diamond Light Source).

References

1. Cowman AF, Crabb BS. Invasion of red blood cells by malaria parasites. Cell. 2006; 124:755–766. [PubMed: 16497586]
2. Tham WH, Healer J, Cowman AF. Erythrocyte and reticulocyte binding-like proteins of *Plasmodium falciparum*. Trends Parasitol. 2012; 28:23–30. [PubMed: 22178537]
3. Baum J, et al. Reticulocyte-binding protein homologue 5 - an essential adhesin involved in invasion of human erythrocytes by *Plasmodium falciparum*. Int. J. Parasitol. 2009; 39:371–380. [PubMed: 19000690]
4. Crosnier C, et al. Basigin is a receptor essential for erythrocyte invasion by *Plasmodium falciparum*. Nature. 2011; 480:534–537. [PubMed: 22080952]
5. Douglas AD, et al. Neutralization of *Plasmodium falciparum* merozoites by antibodies against PfRH5. J. Immunol. 2014; 192:245–258. [PubMed: 24293631]
6. Douglas AD, et al. The blood-stage malaria antigen PfRH5 is susceptible to vaccine-inducible cross-strain neutralizing antibody. Nat. Commun. 2011; 2:601. [PubMed: 22186897]
7. Williams AR, et al. Enhancing blockade of *Plasmodium falciparum* erythrocyte invasion: assessing combinations of antibodies against PfRH5 and other merozoite antigens. PLoS Pathog. 2012; 8:e1002991. [PubMed: 23144611]
8. Bustamante LY, et al. A full-length recombinant *Plasmodium falciparum* PfRH5 protein induces inhibitory antibodies that are effective across common PfRH5 genetic variants. Vaccine. 2013; 31:373–379. [PubMed: 23146673]
9. Reddy KS, et al. Bacterially expressed full-length recombinant *Plasmodium falciparum* RH5 protein binds erythrocytes and elicits potent strain-transcending parasite-neutralizing antibodies. Infect. Immun. 2014; 82:152–164. [PubMed: 24126527]
10. Chen L, et al. An EGF-like protein forms a complex with PfRh5 and is required for invasion of human erythrocytes by *Plasmodium falciparum*. PLoS Pathog. 2011; 7:e1002199. [PubMed: 21909261]
11. Rodriguez M, Lustigman S, Montero E, Oksov Y, Lobo CA. PfRH5: a novel reticulocyte-binding family homolog of *Plasmodium falciparum* that binds to the erythrocyte, and an investigation of its receptor. PLoS ONE. 2008; 3:e3300. [PubMed: 18827878]
12. Manske M, et al. Analysis of *Plasmodium falciparum* diversity in natural infections by deep sequencing. Nature. 2012; 487:375–379. [PubMed: 22722859]
13. Tran TM, et al. Naturally acquired antibodies specific for *Plasmodium falciparum* reticulocyte-binding protein homologue 5 inhibit parasite growth and predict protection from malaria. J. Infect. Dis. 2014; 209:789–798. [PubMed: 24133188]
14. Tham WH, et al. Complement receptor 1 is the host erythrocyte receptor for *Plasmodium falciparum* PfRh4 invasion ligand. Proc. Natl Acad. Sci. USA. 2010; 107:17327–17332. [PubMed: 20855594]
15. Hayton K, et al. Erythrocyte binding protein PfRH5 polymorphisms determine species-specific pathways of *Plasmodium falciparum* invasion. Cell Host Microbe. 2008; 4:40–51. [PubMed: 18621009]
16. Hayton K, et al. Various PfRH5 polymorphisms can support *Plasmodium falciparum* invasion into the erythrocytes of owl monkeys and rats. Mol. Biochem. Parasitol. 2013; 187:103–110. [PubMed: 23305874]
17. Wanaguru M, Liu W, Hahn BH, Rayner JC, Wright GJ. RH5-Basigin interaction plays a major role in the host tropism of *Plasmodium falciparum*. Proc. Natl Acad. Sci. USA. 2013; 110:20735–20740. [PubMed: 24297912]

18. Higgins MK, Carrington M. Sequence variation and structural conservation allows development of novel function and immune evasion in parasite surface protein families. Protein Sci. 2014; 23:354–365. [PubMed: 24442723]
19. Hirose S, Shimizu K, Kanai S, Kuroda Y, Noguchi T. POODLE-L: a two-level SVM prediction system for reliably predicting long disordered regions. Bioinformatics. 2007; 23:2046–2053. [PubMed: 17545177]
20. Miura K, et al. Anti-apical-membrane-antigen-1 antibody is more effective than anti-42-kilodalton-merozoite-surface-protein-1 antibody in inhibiting plasmodium falciparum growth, as determined by the in vitro growth inhibition assay. Clin. Vaccine Immunol. 2009; 16:963–968. [PubMed: 19439523]
21. Sheehy SH, et al. Phase Ia clinical evaluation of the *Plasmodium falciparum* blood-stage antigen MSP1 in ChAd63 and MVA vaccine vectors. Mol. Ther. 2011; 19:2269–2276. [PubMed: 21862998]
22. Battye TG, Kontogiannis L, Johnson O, Powell HR, Leslie AG. iMOSFLM: a new graphical interface for diffraction-image processing with MOSFLM. Acta Crystallogr. D Biol. Crystallogr. 2011; 67:271–281. [PubMed: 21460445]
23. Leslie AG. The integration of macromolecular diffraction data. Acta Crystallogr. D Biol. Crystallogr. 2006; 62:48–57. [PubMed: 16369093]
24. Evans, PR. In: Sawyer, L.; Isaacs, N.; Bailey, S., editors. Data reduction; Proceedings of the CCP4 Study Weekend; Daresbury Laboratory, Warrington, UK. 1993; p. 114-122.
25. Winn MD, et al. Overview of the CCP4 suite and current developments. Acta Crystallogr. D Biol. Crystallogr. 2011; 67:235–242. [PubMed: 21460441]
26. McCoy AJ, et al. Phaser crystallographic software. J. Appl. Crystallogr. 2007; 40:658–674. [PubMed: 19461840]
27. Zhang KY, Cowtan K, Main P. Combining constraints for electron-density modification. Methods Enzymol. 1997; 277:53–64. [PubMed: 18488305]
28. Cowtan K. The Buccaneer software for automated model building. Acta Crystallogr. D Biol. Crystallogr. 2006; 62:1002–1011. [PubMed: 16929101]
29. Murshudov GN, et al. REFMAC5 for the refinement of macromolecular crystal structures. Acta Crystallogr. D Biol. Crystallogr. 2011; 67:355–367. [PubMed: 21460454]
30. Bricogne, G., et al. BUSTER version 2.10.0. Global Phasing Ltd.; Cambridge, UK: 2011.
31. Emsley P, Lohkamp B, Scott WG, Cowtan K. Features and development of Coot. Acta Crystallogr. D Biol. Crystallogr. 2010; 66:486–501. [PubMed: 20383002]
32. Laskowski RA, MacArthur MW, Moss DS, Thornton JM. PROCHECK - a program to check the stereochemical quality of protein structures. J. App. Cryst. 1993; 26:283–291.
33. Sievers F, et al. Fast, scalable generation of high-quality protein multiple sequence alignments using Clustal Omega. Mol. Syst. Biol. 2011; 7:539. [PubMed: 21988835]
34. Gouet P, Courcelle E, Stuart DI, Metoz F. ESPript: analysis of multiple sequence alignments in PostScript. Bioinformatics. 1999; 15:305–308. [PubMed: 10320398]
35. Kelley LA, Sternberg MJE. Protein structure prediction on the Web: a case study using the Phyre server. Nat. Protoc. 2009; 4:363–371. [PubMed: 19247286]
36. Konarev PV, Volkov VV, Sokolova AV, Koch MHJ, Svergun DI. PRIMUS: a Windows PC-based system for small-angle scattering data analysis. J. Appl. Crystallogr. 2003; 36:1277–1282.
37. Petoukhov MV, Konarev PV, Kikhney AG, Svergun DI. ATSAS 2.1 - towards automated and web-supported small-angle scattering data analysis. J. Appl. Crystallogr. 2007; 40:S223–S228.
38. Guinier, A.; Fournet, G. Small-angle Scattering of X-rays. John Wiley and Sons; New York, USA: 1955.
39. Porod, G. General Theory Small Angle X-ray Scattering. Academic Press, Inc.; London, UK: 1982.
40. Franke D, Svergun DI. DAMMIF, a program for rapid ab-initio shape determination in small-angle scattering. J. Appl. Crystallogr. 2009; 42:342–346.
41. Konarev PV, Petoukhov MV, Volkov VV, Svergun DI. ATSAS 2.1, a program package for small-angle scattering data analysis. J. Appl. Crystallogr. 2006; 39:277–286.

42. Kozin MB, Svergun DI. Automated matching of high- and low-resolution structural models. J. Appl. Crystallogr. 2001; 34:33–41.
43. Birmanns S, Rusu M, Wriggers W. Using Sculptor and Situs for simultaneous assembly of atomic components into low-resolution shapes. J. Struct. Biol. 2011; 173:428–435. [PubMed: 21078392]
44. Schuck P. Size-distribution analysis of macromolecules by sedimentation velocity ultracentrifugation and Lamm equation modeling. Biophys. J. 2000; 78:1606–1619. [PubMed: 10692345]
45. Schuck P, Perugini MA, Gonzales NR, Howlett GJ, Schubert D. Size-distribution analysis of proteins by analytical ultracentrifugation: Strategies and application to model systems. Biophys. J. 2002; 82:1096–1111. [PubMed: 11806949]
46. Laue, TM.; Shah, BD.; Ridgeway, TM.; Pelletier, SL. Analytical Ultracentrifugation in Biochemistry and Polymer Science. Harding, S.; Rowe, A., editors. Royal Society of Chemistry; Cambridge, UK: 1992. p. 90-125.
47. Vistica J, et al. Sedimentation equilibrium analysis of protein interactions with global implicit mass conservation constraints and systematic noise decomposition. Anal. Biochem. 2004; 326:234–256. [PubMed: 15003564]

Europe PMC Funders Author Manuscripts

Europe PMC Funders Author Manuscripts

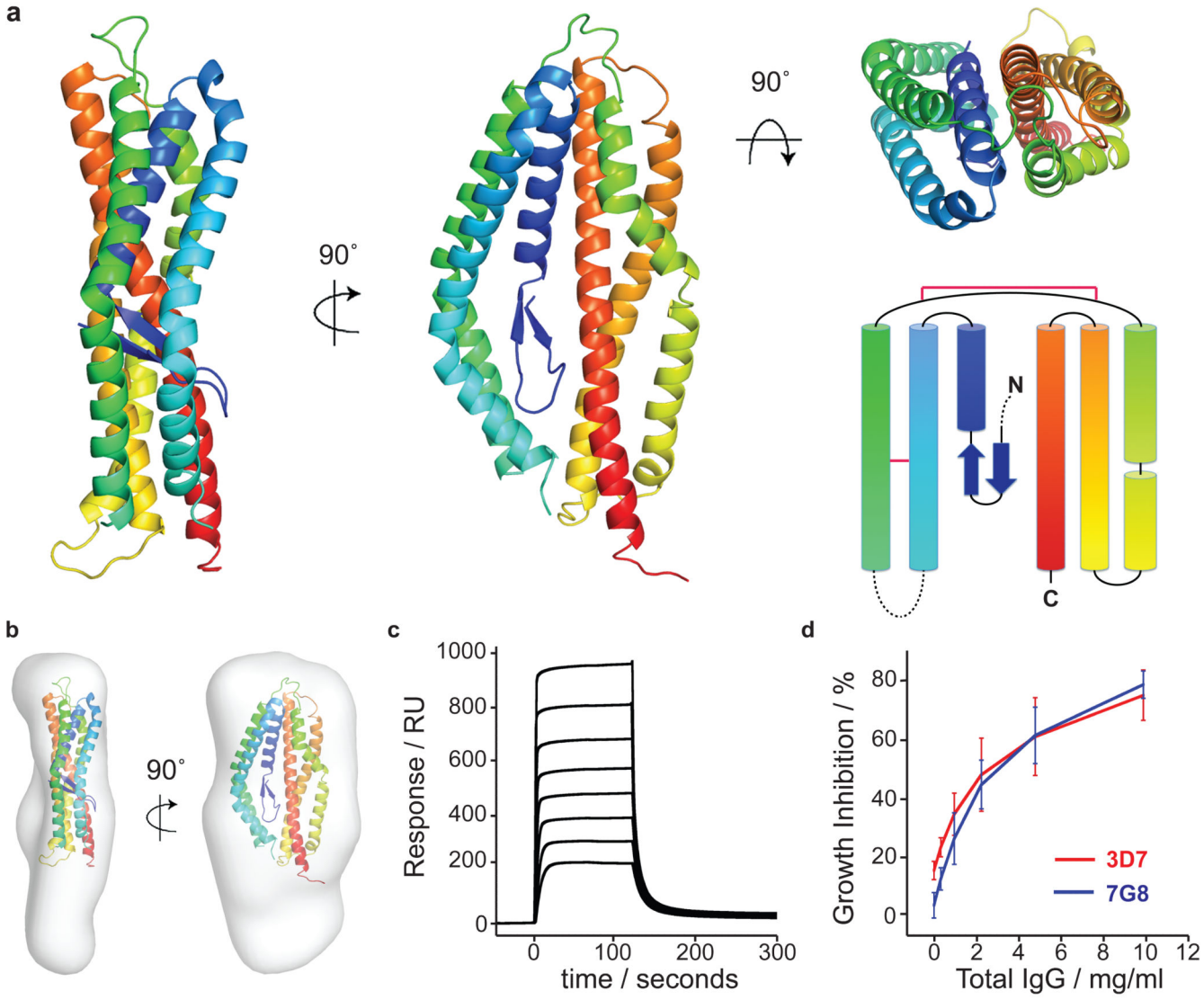

Figure 1. The structure of PfRH5

a, Three views of PfRH5ΔNL (from the PfRH5ΔNL:9AD4 structure), and a schematic topology diagram, coloured in rainbow from blue (N-terminus) to red (C-terminus). Disulphide bonds are indicated on the topology diagram by red lines. **b**, PfRH5ΔNL structure docked into a SAXS envelope of full-length PfRH5. **c**, SPR analysis of the PfRH5ΔNL:basigin interaction. **d**, *In vitro* growth inhibition activity (GIA) of IgG from rabbits immunised with PfRH5ΔNL against 3D7 (red) and 7G8 (blue) *P. falciparum* strains. The error bars are standard error of mean (n=3).

Europe PMC Funders Author Manuscripts

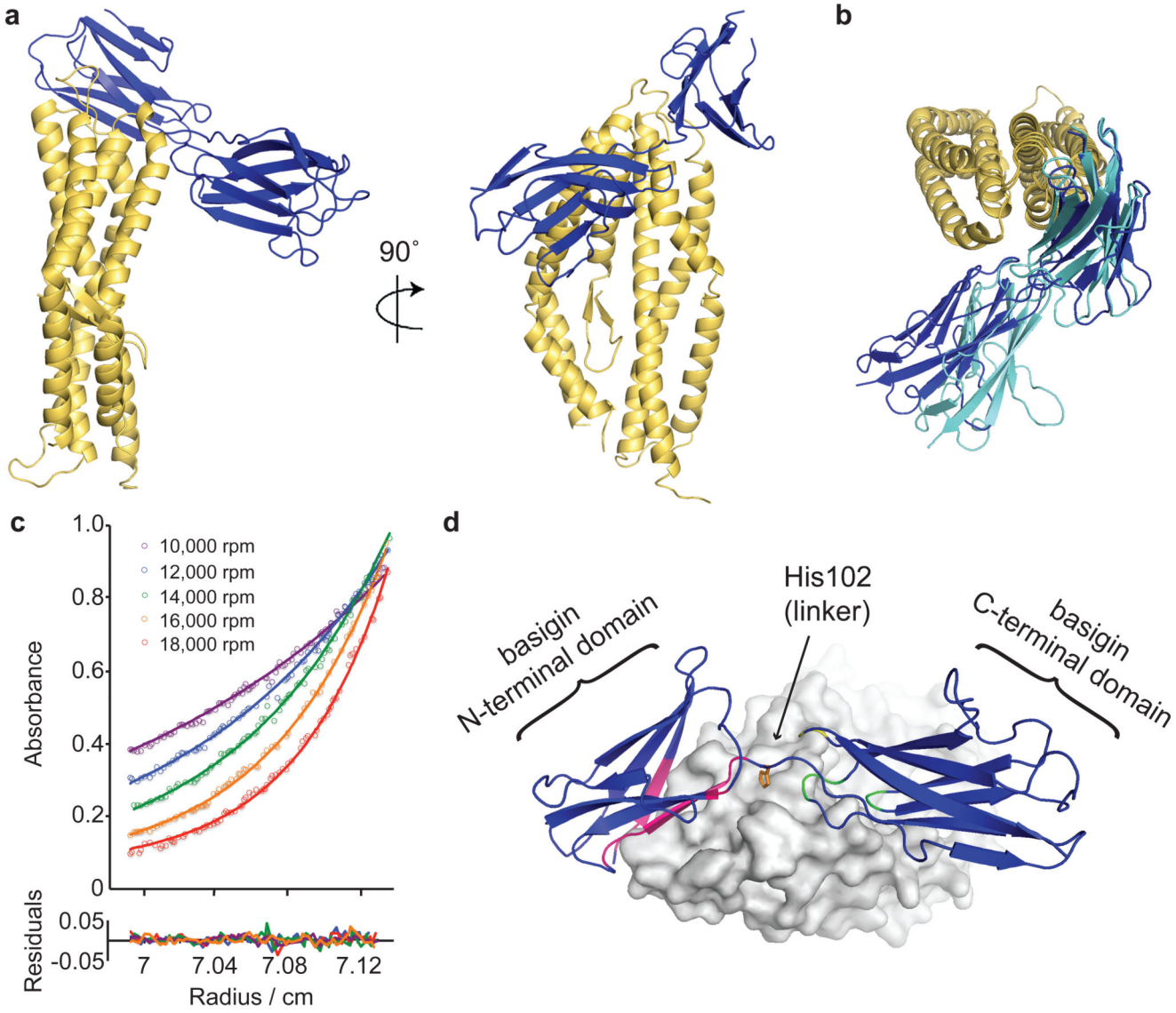

Figure 2. The structure of the PfRH5:basigin complex

a, The structure of PfRH5ΔNL (yellow) bound to basigin (blue). **b**, A top view of the PfRH5ΔNL:basigin complex showing the two conformations of basigin (blue and cyan) found in the asymmetric unit, aligned on PfRH5ΔNL. **c**, Equilibrium analytical ultracentrifugation analysis of PfRH5:basigin indicating a 1:1 complex. **d**, Close-up of the PfRH5:basigin binding site. Basigin residues in the N-terminal domain (pink), the linker (His102, orange stick), and the C-terminal domain (green) contact PfRH5 (grey surface). In the alternative basigin conformation in the asymmetric unit, the cyan loop contacts PfRH5.

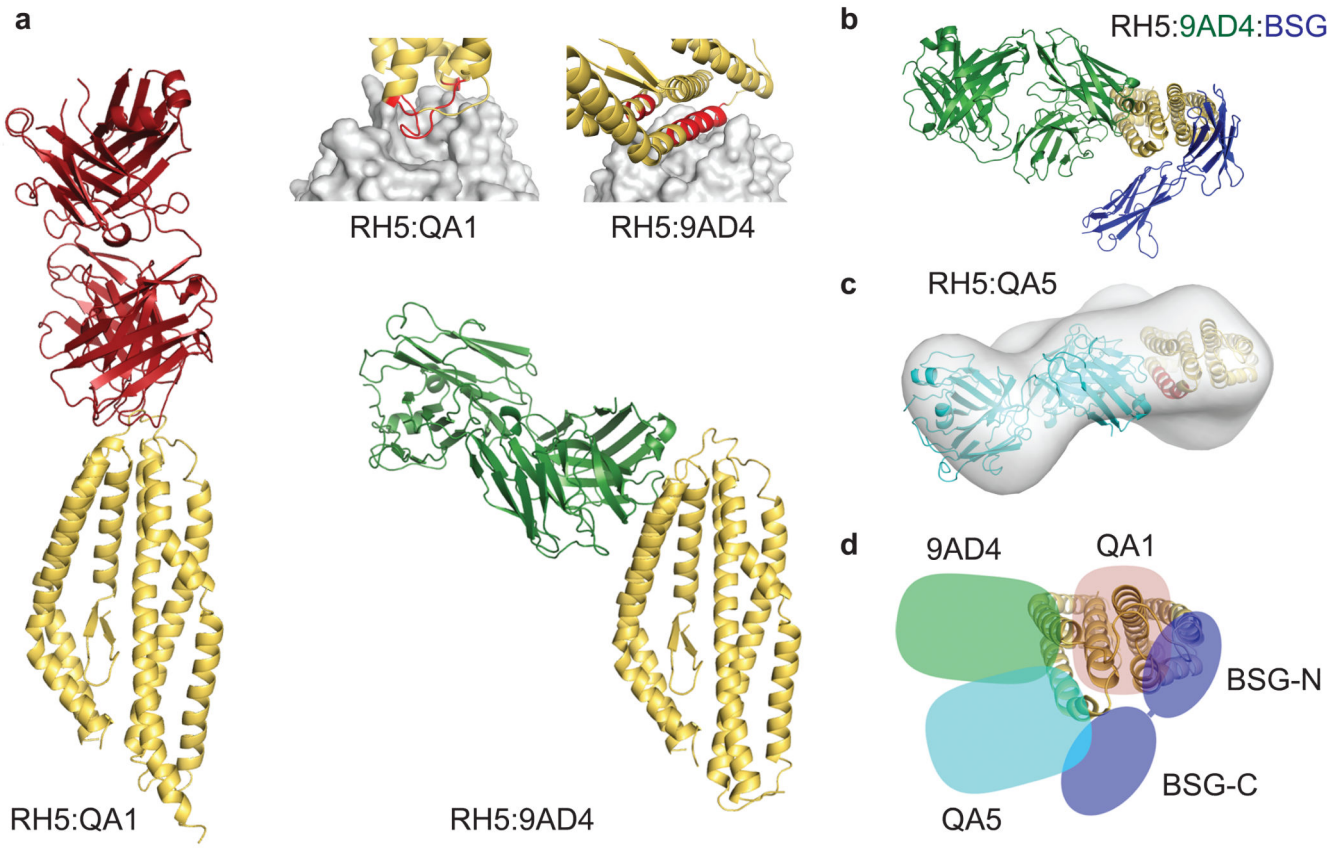

Figure 3. Structural analysis of binding of invasion-inhibitory antibody fragments to PfRH5

a, Crystal structures of PfRH5ΔNL (yellow) bound to inhibitory antibody fragments QA1 (red) and 9AD4 (green). Close-up views of the PfRH5 epitopes (red) are shown with antibodies as grey surfaces. **b**, Top view of PfRH5ΔNL:9AD4 crystal structure with superimposed basigin (blue) aligned on PfRH5. **c,** Top view of a model of PfRH5:QA5, in a SAXS-derived envelope, with the putative QA5 epitope highlighted red[5]. **d**, Schematic showing binding sites for the N- and C-terminal domains of basigin (BSG-N and BSG-C; blue), QA1 (red), 9AD4 (green) and QA5 (cyan), on the structure of PfRH5ΔNL.

Europe PMC Funders Author Manuscripts